PHYSICAL REVIEW D **85,** 103009 (2012)

Multi-GeV neutrino emission from magnetized gamma-ray bursts

Shan Gao and Peter Mészáros

Department of Physics, Department of Astronomy and Astrophysics, Center for Particle Astrophysics, The Pennsylvania State University, University Park, 16802, USA

(Received 23 December 2011; revised manuscript received 18 March 2012; published 29 May 2012)

We investigate the expected neutrino emissivity from nuclear collisions in a magnetically dominated model of gamma-ray bursts motivated by recent observational and theoretical developments. The results indicate that small multi-GeV neutrino fluxes are expected for model parameter values which are typical of electromagnetically detected bursts. We show that for detecting at least one muon event in IceCube and its DeepCore subarray, a single burst must be near the high end of the luminosity function, and at low redshifts $z \lesssim 0.1$, where the burst rate is very low. We also calculate the luminosity and distance ranges which can generate 0.01–1 muon events per gamma-ray burst in the same detectors, which may be of interest if simultaneously detected electromagnetically, or if measured with future extensions of IceCube or other neutrino detectors with larger effective volume and better sensitivity.

DOI: 10.1103/PhysRevD.85.103009 PACS numbers: 95.85.Ry

I. INTRODUCTION

Observations of multi-GeV photons from gamma-ray bursts (GRB) recently accumulated by the Fermi satellite (e.g. Ref. [1,2]) have pointed out the need to reevaluate the type of models used to explain the prompt photon emission mechanisms and the location of the emission regions in these objects (e.g. Ref. [3]). In particular, concerns about the radiative efficiency of usual internal shock models and the larger radii required to avoid two-photon degradation of the spectra have spurred the investigation of baryonic (non-MHD) jet models where the radiation arises in a jet photosphere [4–6]. In such baryon-loaded jet models, at a certain radius, the time scale of the nuclear elastic collisions (which couple the proton p and neutron n components) becomes longer than the expansion time scale, i.e. the collision optical depth falls below $o(1)$, and the two components decouple from each other [7,8]. The protons can continue to be accelerated by the radiation, while the neutrons, which have zero electric charge, start to coast with a constant Lorentz factor. Starting at this decoupling radius and for some distance beyond, the longitudinal drift velocity between the n and p becomes $\Delta v \gtrsim 0.5c$, and they start to collide inelastically. Such large relative velocities between n and p components also can arise in realistic jets where the bulk Lorentz factor Γ depends on the polar angle θ, which also leads to inelastic collisions [6,9], as neutrons from the outer parts (sheath) of the jet thermally drift into the jet core. In both pictures, pions are created, which in the case of the dynamics being dominated by the baryons, results in multi-GeV photons and neutrino production [6,8].

A different approach towards resolving the radiative efficiency of GRBs involves consideration of magnetically dominated jets [10–12]. Some of these magnetic models assume an almost baryon-free outflow [12–16], while in other cases, a substantial but dynamically subdominant baryon load is assumed [10,11,17–22]. The baryons in such jet models are expected to accelerate at a different rate than in baryonic (non-MHD) jet models, and the different dynamics leads to quantitatively different predictions for the photon spectrum [23]. Similarly, it should lead to quantitatively different neutrino spectra, which we investigate in this paper.

Unlike in the previous investigations cited above, here, we consider the neutrino spectra arising from nuclear collision effects in magnetically dominated GRB outflows. In this case, both the radial np decoupling radius as well as the photosphere occur at larger radii from the central engine than in the nonmagnetic case, and also the transverse drift of neutrons from the periphery of the jet into the jet core becomes important at different radii, where the physical conditions differ from those previously considered. As a consequence, multi-GeV photons are produced at somewhat softer energies and with appreciable time delays [23] respect to the MeV photospheric photons, but the detailed neutrino spectrum for such magnetically dominated jets has not been considered so far. In this paper, we investigate numerically the neutrino spectrum expected in magnetically dominated baryon-collisional GRB models, taking into account both longitudinal and transverse n, p decoupling and inelastic collisions. These neutrinos are in the energy sensitivity range of IceCube and its DeepCore [24–26] subarray.

In Sec. II, we briefly introduce the astrophysical model and present the method of neutrino emission calculation. In Sec. III, we present the results for the expected neutrino fluxes and muon events, as well as the detection prospects with DeepCore and IceCube. A discussion and summary of the results is given in Sec. IV.

II. THE NUCLEAR COLLISION SCENARIOS

We consider two types of nuclear collision scenarios, one where the collisions occur as a result of longitudinal

(radial) velocity drifts, and another where they occur as result of transverse (relative to the jet axis) drifts of neutrons from an outer jet sheath to an inner jet core where the bulk Lorentz factor is different. We consider both of these cases in the context of magnetically dominated jet dynamics, which differs from the usually considered baryonically dominated dynamics.

A. Neutrinos from longitudinal nuclear collisions

In a magnetized outflow, the bulk Lorentz factor accelerates initially as [27–29]

$$\Gamma = \begin{cases} (r/r_0)^{1/3} & r < r_{\rm sat} \\ \eta & r > r_{\rm sat} \end{cases}, \tag{1}$$

where $r_{\rm sat} = \eta^3 r_0$ is the saturation radius beyond which the jet material starts to coast. (This is in contrast to the baryonic-dominated dynamics, where $\Gamma \propto r$ up to an $r_{\rm sat} \sim \eta r_0$).

At the radius where the comoving baryon collision time scale becomes longer than the adiabatic expansion time scale, the protons decouple from the neutrons, and they continue to accelerate as $\Gamma \propto r^{1/3}$. The condition above is expressed as

$$t'_{\rm exp} = r/c\Gamma < t'_{\rm col} = 1/n'_b \sigma_\pi c, \tag{2}$$

where

$$n'_b = L_{\rm tot}/4\pi r^2 c \eta \Gamma m_p c^2 \tag{3}$$

is the total comoving baryon density in the flow, $L_{\rm tot}$ is the jet total isotropic equivalent luminosity, and $\eta = L_{\rm tot}/\dot{M}c^2$ is the dimensionless entropy or energy-to-mass outflow ratio.

The neutrons thereafter coast with a bulk Lorentz factor $\Gamma_n = (r_d/r_0)^{1/3}$, where

$$r_d = \eta_\pi^3 (\eta_\pi/\eta)^{3/5} r_0 \tag{4}$$

is the decoupling radius $r_d \approx r_\pi$ defined from the condition (2) (see also Ref. [12]). Here, η_π is a dimensionless parameter given by

$$\eta_\pi = \left(\frac{L_{\rm tot}\sigma_\pi}{4\pi c m_p c^2 r_0}\right)^{1/6} \approx 1.33 \times 10^2 L_{54}^{1/6} r_{0,7}^{-1/6}, \tag{5}$$

where $\sigma_\pi \sim 3 \times 10^{-26}$ cm^{-2}. Decoupling occurs at $r_d < r_{\rm sat}$ if $\eta > \eta_\pi$; otherwise, if the condition (2) is met at a radius above $r_{\rm sat}$, decoupling never happens and the p and n just coast together.

Beyond the decoupling radius, the accelerated protons collide longitudinally[1] with the neutrons, which have a smaller Lorentz factor. The collisions become mostly inelastic when their relative Lorentz factor $\Gamma_{\rm rel} \gtrsim 1.3$; see Eq. (8). In the star frame, each shell encompassed within $(r, r + dr)$ contributes to the pionization optical depth for those protons by an amount

$$d\tau(r) = n_n(r)\Delta\beta\sigma_\pi dr, \tag{6}$$

where $\Delta\beta$ is the relative speed between protons and neutrons in the lab frame, $\Delta\beta = [1 - \Gamma^{-2}(r)]^{1/2} - [1 - \Gamma^{-2}(r_d)]^{1/2}$.

To estimate the pion spectrum, we can, for simplicity, assume that for each collision, in the center-of-mass frame, the proton and neutron are approximately at rest after the collision, with a maximum number of pions created, which are also approximately at rest (we will use a more detailed treatment in Sec. II B). Therefore, the invariant energy is

$$\sqrt{s} = \sqrt{(p_p^\mu + p_n^\mu)^2} = \sqrt{2(1 + \Gamma_{\rm rel})}, \tag{7}$$

where the proton Lorentz factor viewed in neutron comoving frame is

$$\Gamma_{\rm rel} = \frac{1}{2}\left(\frac{\Gamma_p}{\Gamma_n} + \frac{\Gamma_n}{\Gamma_p}\right). \tag{8}$$

This relation is valid when both $\Gamma_p, \Gamma_n \gg 1$.

The maximum number of pions which can be created (the pion multiplicity) is

$$\lambda_\pi = \left(\sqrt{2(1 + \Gamma_{\rm rel})} - 2\right)/(m_\pi/m_p), \tag{9}$$

with a Lorentz factor

$$\Gamma_\pi(r) = \frac{\Gamma_p(r) + \Gamma_d}{\sqrt{2[1 + \Gamma_{\rm rel}(r)]}}. \tag{10}$$

The radius-dependent probability for a proton to interact with a neutron is

$$P(r) = e^{-\tau(r)}, \tag{11}$$

where $\tau(r) = \int_{r_d}^{r} d\tau$ and $d\tau(r)$ is given by Eq. (6). The number of pions created per proton is

$$N_\pi = \int_{r_d}^{r_{\rm max}} \lambda_\pi dP(r), \tag{12}$$

where the maximum interaction radius is estimated as $r_{\rm max} \sim c t_{\rm duration}/\Delta\beta \sim 3 r_{\rm sat}$. (The last equality is for the choice of nominal parameters in MR11. Otherwise $r_{\rm max} \sim c t_{n-{\rm decay}} \Gamma_n$).

Beyond the decoupling radius r_d, the protons continue to be accelerated until reaching $r_{\rm sat}$. When the energy is above the threshold to create one pion in a collision with a neutron, we define this radius as, e.g., r_1. At a larger radius, protons with greater energies create more pions per collision. The pion Lorentz factor as a function of their production radius is given by Eq. (10). The inelastic interactions start from r_1 and may last to a radius above $r_{\rm sat}$. Beyond $r_{\rm sat}$, the protons coast with a Lorentz factor η and

[1]...neglecting random thermal motions and transverse collisions, which are discussed in the next section.

(provided $\eta > \eta_\pi$) create pions with a monochromatic energy (in the first-order approximation used in this section). In fact, the resulting neutrino spectrum, after the pions decay, will be broadened due to various factors (e.g. a) thermal motions of both protons and neutrons; b) energy dispersion of the created charged pions; c) kinematics of the pion and muon decay process; d) pion and muon cooling and rescattering). In this Sec. II A, the above four factors are not considered in the calculation, except in a qualitative way. This is adequate because, as discussed in Sec. II B and in Fig. 1, it turns out that the dominant process for neutrino production is through transverse nuclear collisions. As an example, for a case with $\eta = 500$, $r_0 = r_{0,7}$, $L_{\rm tot} = L_{54}$, $L_p = L_n = 0.5L_b$ (where the subindex p, n, b refer to proton, neutron, and baryon luminosity, respectively), the charged pion spectrum from longitudinal nuclear collision is shown in Fig. 1. For simplicity reasons, a Gaussian distribution is assumed to represent the dispersion. The pion spectrum from transverse collisions is also shown in the figure, anticipating the results of the more detailed treatment of the latter in Sec. II B and after.

B. Neutrinos from transverse nuclear collisions

In more realistic jet models, the jet properties vary in the transverse (θ) direction. Hydrodynamical simulations indicate a smaller Lorentz factor in the jet outer regions (jet edge) than that in the jet core [30], and qualitatively similar results appear also in some MHD outflows [31]. As a simple ideal model, we consider the transverse structure of the jet in the region outside the star to be represented by a two-step function, consisting of an inner jet core with Γ give by Eq. (1) and a slower outer jet, or jet sheath, with a saturation Lorentz factor of $\eta_{\rm out} = 10^2\eta_{\rm out,2}$. Both inner and outer jets will have been populated with protons and free neutrons already near the black hole, where any nuclei present would have been photodissociated. Because of thermal diffusion, neutrons in the jet sheath can drift sideways into the jet core and interact with baryons in the core. For significant effects, this requires the neutrons in the jet sheath to drift through a substantial transverse distance $\sim r\theta$ into the core. This condition can be roughly estimated as

$$r_\perp \gtrsim \eta_\pi^6\theta < \Gamma_{\rm rel} > r_0/\eta, \tag{13}$$

where $\langle\Gamma_{\rm rel}\rangle$ is the average relative Lorentz factor between the neutron and the baryons encountered along its path.[2] We estimate the number of neutrons which have drifted into the core in a time scale $t_\perp$ (all measured in the star frame) as

$$N_\perp(t_\perp) \sim \pi r^2\theta \int_0^{t_\perp} \phi_n(t)dt, \tag{14}$$

where the diffusive flux $\phi_n(t)$ is from Eq. (14) in MR11. Meanwhile, the number of baryons (n and p) passing longitudinally through the jet core is

$$N_\parallel(t_\perp) \sim \pi r^2\theta n_b ct. \tag{15}$$

The number of collisions *per baryon* in the core is roughly $N_\perp/N_\parallel$, because the pionization optical depth is $\tau \sim 1$ for those neutrons. (The case $N_\perp/N_\parallel \gg 1$ is less likely for typical jet parameters and would involve protons in the core undergoing multiple scatterings resulting in cascades, which is beyond the scope of this paper). From the equations above,

$$N_\perp/N_\parallel \sim 2\eta_{\rm out}^{-1}\eta_\pi^{-3}(1 - T'^{-2})^{1/2}(y\eta/t_\perp)^{1/2}r_\perp, \tag{16}$$

where $r_\perp$ is expressed in units of r_0 and T' is the comoving temperature in units of m_pc^2 ($T' \approx o(1)$ in this case, see MR11). The parameter y is the ratio of neutron density in the sheath to baryon density in the core, $y \equiv n_{n,\rm out}/n_b$, in the star frame.

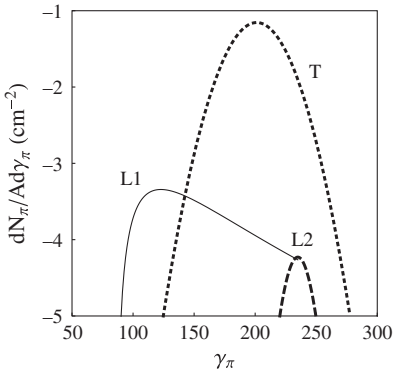

FIG. 1. Charged pion spectrum at the source from longitudinal and transverse nuclear collisions (analytical approximation), normalized to the Earth observer frame. The charged pions decay in the source and are observed at Earth only via their neutrino decay products. The component L1 is from longitudinal pn collisions at radii $r_d < r < r_{\rm sat}$, while the component L2 arises at $r > r_{\rm sat}$. The component T is from transverse drift pn collisions (see Sec. II B). A Gaussian dispersion is assumed for simplicity to represent the broadening of the real spectrum arising from various effects (see Sec. II A). The dominant pion (and neutrino) production comes from the transverse pn collisions, as discussed in Sec. II B. We assume a source with $L_\gamma = 0.1L_{\rm tot} = 10^{53}$ erg/s, $\eta = 500$, $\theta_{\rm jet} = 0.01$ and $z = 0.1$ (see Sec. II C).

[2]The path calculation is a well-defined but complicated problem. To derive Eq. (13), we set the pionization optical depth $\tau_\pi = 1$ along the neutron path for which its transverse displacement amounts to $r\theta$. The path itself is not transverse to the jet axis, due to relativistic beaming according to different sheath and core bulk velocities. $\langle\Gamma_{\rm rel}\rangle$ depends on the details of the jet transverse structure, and the density along the neutron path varies due to the jet dynamics. However, Eq. (13) serves as a rough estimate.

C. Parameters of the model

The neutrino spectrum at Earth depends on a number of parameters. Among these are the total luminosity $L_{\rm tot}$ of the jet, which is initially mostly in magnetic form; the "baryon" luminosity L_b, which is the dominant energy form beyond the saturation radius $r_{\rm sat} = \eta^3 r_0$ (the ratio of these two being defined as $\epsilon_b = L_b/L_{\rm tot}$); and the photon luminosity produced by dissipation process around the photosphere $L_{\rm ph}$ (whose ratio to the total initial luminosity is defined as $\epsilon_{\rm ph} = L_{\rm ph}/L_{\rm tot}$). In the inner jet core, the proton and neutron luminosity are assumed, for simplicity, to be $L_p = L_n = (1/2)L_b$ throughout the paper.[3] We take for the ratio y of baryon density in the outer jet to that in the inner jet a nominal value $y = 0.01$. The discussions on results from different $\eta_{\rm core}$ and $\eta_{\rm out}$ are presented in Figs. 2 and 3. We adopt a nominal jet opening angle of $\theta = 0.01$, other values being discussed in Fig. 4. We also adopt as a standard burst duration in the source frame a value of $t = 20$ s, which is a rough average value for long bursts. The redshift-distance relation used is that for a standard ΛCDM cosmology.

III. GEV NEUTRINOS AND THEIR DETECTABILITY IN DEEPCORE AND ICECUBE

A. Neutrinos from a single GRB

The neutrinos are produced by nuclear collisions between protons and neutrons leading to pions, the charged pions subsequently decaying[4] as

$$\pi^{\pm} \rightarrow \mu^{\pm} + \nu_{\mu}(\bar{\nu}_{\mu}) \rightarrow e^{\pm} + \nu_e(\bar{\nu}_e) + \nu_{\mu} + \bar{\nu}_{\mu}. \quad (17)$$

The neutrino flavor mix produced at the source is determined by Eq. (17), but as a result of neutrino oscillations, the neutrino flavor received at Earth depends on energy and distance. Since, in this paper, we discuss the general case, not a specific GRB, we approximate the received neutrino flux as having equal numbers in all three flavors.

To calculate the neutrino spectrum from nuclear collisions, the use of a numerical code is desirable. The commonly used PHYTIA-8 code uses a minimum threshold energy of $E_{cm} = 10$ GeV, which for the energies considered here, leads to inaccuracies. For this reason, we have used two different numerical methods. One method uses the publicly available code of Ref. [32]. These authors use a parametrization formula for γ, $e^{\pm}$, ν, and $\bar{\nu}$ which is

[3]The outer jet neutrons can also collide with jet core neutrons and produce neutrinos. However, the relative Lorentz factor with neutrons is smaller than that with the accelerated protons in the jet core, so the neutrino production through nn collisions is less efficient than for pn collisions. Only the latter are discussed in this paper.

[4]The charged Kaon leading decay channel is similar and can be approximated as effective pions. However, the number ratio of Kaons to pions produced by hadron collision at these energies is less than 0.1 and can be neglected for the purpose of this paper.

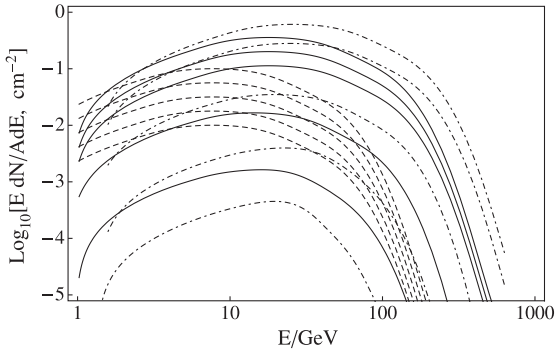

FIG. 2. The $\nu_{\mu} + \bar{\nu}_{\mu}$ fluence in the Earth observer frame from a single burst, integrated over the outburst duration, for a nominal redshift of $z = 0.1$. The other nominal parameters are the same as in Fig. 1, except for $\eta_{\rm core} = 10\eta_{\rm out} = 300$, 700, 1000, indicated with dashed, solid and dotted-dashed lines, respectively. The lines in each style are arranged from top to bottom in the sequence $L_{\rm tot} \sim L_b = 10^{55}$, $10^{54.5}$, 10^{54}, $10^{53.5}$, 10^{53} erg/s.

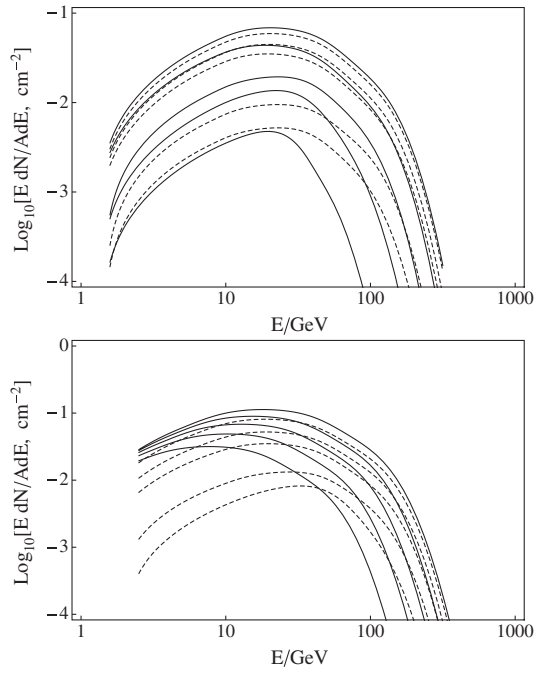

FIG. 3. The $\nu_{\mu} + \bar{\nu}_{\mu}$ fluence in the Earth observer frame from $z = 0.1$ for different parameters. Top panel: solid lines from bottom to top are for $\eta_{\rm core} = 300$, 400, 500, 600, 700; dashed lines from bottom to top are for $\eta_{\rm core} = 2000$, 1500, 1000, 900, 800, with a fixed $\eta_{\rm out} = 100$. Bottom panel: solid lines, bottom to top are $\eta_{\rm core} = 300$, 400, 500, 600, 700; dashed lines, bottom to top are $\eta_{\rm core} = 1500$, 1200, 1000, 900, 800 with a running $\eta_{\rm out} = 0.1\eta_{\rm core}$. Both panels are for $L_p = 10^{54}$ erg/s, the value of $\eta_{\rm core}$ yielding the largest neutrino flux being around $\eta \sim 700$. When $\eta_{\rm core}$ approaches 300, the pion multiplicity becomes smaller due to a smaller relative Lorentz factor between outer and inner jet particles [top figure, Eq. (9)] or due to a slightly smaller diffusion rate [Eq. (16)]. For very high $\eta_{\rm core} \gtrsim 10^3$, the pion multiplicity similarly decreases.

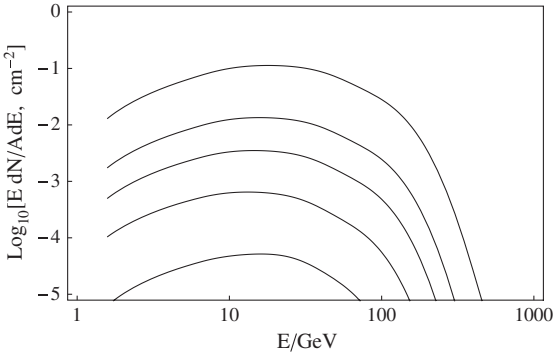

FIG. 4. The $\nu_\mu + \bar{\nu}_\mu$ number fluence in the Earth observer frame from $z = 0.1$, calculated for $\eta_{\rm core} = 10\eta_{\rm out} = 700$, $L_T \sim L_b = 10^{54}$ erg/s for various jet opening angles $\theta_{\rm jet} = 0.01$, 0.02, 0.03, 0. 04, 0.05, 0.1 (top to bottom).

carried out separately for diffractive and nondiffractive processes and resonance-excitation processes, with a logarithmic rising pp inelastic cross section with T_p. The secondary particle spectra are initially extracted out of events generated for monoenergetic protons (0.488 GeV $< T_p <$ 512 TeV), using several simulation programs. The spectra are then fitted by a common parametrized function, separately for the physical processes listed above. Finally, the parameters determined for monoenergetic protons are fitted as a function of proton energy. The procedure was repeated for all those secondary particle types mentioned above. In order to approximate better the experimental data at lower energies, two baryon resonance contributions have been included, one representing the $\Delta(1232)$ and the other representing multiple resonances around 1600 MeV$/c^{-2}$. However, as pointed out also by Ref. [32], the pion mean energy in this code is slightly underestimated at incident proton kinetic energy (in the fixed target lab frame) of $T_p \sim 2$ GeV and above, compared to experimental data. Therefore, in this paper, we have corrected this discrepancy by multiplying the resultant neutrino energy by a factor of 1.3 using an approximate fit to the Fig. 5 of their paper. This causes a slightly overestimated pion mean energy near the threshold energy $T_p \sim 0.3$ GeV; however, this energy range is not of interest for our purposes in this paper, since it results in a nondetectable neutrino at the associated energy. We refer to this numerical calculation as method A.

We have also developed a different code, which is independent of method A, in order to cross-check the validity of method A around energies $T_p \gtrsim 4$ GeV and in order to gain better transparency on the underlying physical processes where this is not otherwise made explicit in method A. We refer to this second method as method B. The energy $T_p \gtrsim 4$ GeV is of particular importance here for at least three reasons: i) it arises naturally in the astrophysical model considered here; ii) nuclei in this range can produce substantial neutrino fluxes; and iii) IceCube and its DeepCore subarray neutrino detectors are sensitive to the details of the neutrino spectrum in the energy range 10–1000 GeV. In method B, the charged pion spectrum is approximated by a radial scaling [33], based on the apparent Feynman scaling violation at $x_R \equiv E/(\sqrt{s}/2) \ll 1$. The meson decay kinematics are well-established, and in method B, we follow the formulation of Ref. [34].[5]

A comparison of the muon neutrino and antineutrino spectra at the source calculated using methods A and B is plotted in Fig. 5, for an incident proton energy $T_p =$ 3.8 GeV. It is seen that the two results agree well with each other. We note that:

(i) both methods would result in a very small number of neutrinos which violate energy-momentum conservation. Although the total amount of energy involved in these neutrinos is well below a fraction $\sim 10^{-3}$, and thus negligible, we have nonetheless applied a cutoff in the spectrum beyond the energy where this occurs for both methods A and B.

(ii) both these methods simulate pp collisions, instead of pn collisions. For pp collisions, the π^+ multiplicity is therefore greater than that of π^- due to charge conservation near the pion creation threshold energy. At $\sqrt{s}\sim$ few GeV or higher, the two multiplicities tend to equal each other.

In method A we sum the neutrino and antineutrino from both π^+ and π^- channels. In method B, Hillas used one fitted formula to describe both π^+ and π^- spectra. Thus, for the summed neutrino and antineutrino spectrum resulting from the decay products of these mesons, the discrepancy between pp and pn collisions becomes less noticeable.

The muon neutrino and antineutrino differential number fluence at Earth for a single burst (neutrinos per energy decade, integrated over the duration of the outburst) is shown, after oscillations, in Figs. 2–4. In Figs. 2 and 3, we note a saturation effect in the dependence of L_ν on L_p: at low L_p, L_ν grows fast with it and then stabilizes above $L_p \sim 10^{54}$ erg/s. This effect is mainly due to the change of relative Lorentz factors between $\eta_{\rm core}$ and $\eta_{\rm out}$ by choices of different astrophysical parameters. $\Gamma_{\rm rel}$ grows with L_p if we fix other parameters and saturates at some $L_{p,0}$ level (may be already saturated at the low end of L_p in parts of our parameter space). A higher $\Gamma_{\rm rel}$ is associated with more secondary leptons (including neutrinos) per pn collision. However, when saturated, the received neutrino flux grows at a slower rate with L_p because the increase of fluence is then only due to the fact that we have more protons in the jet.

[5]Noting a typo in this reference, where in his Eq. [14], second line, η_ν should be replaced by ξ.

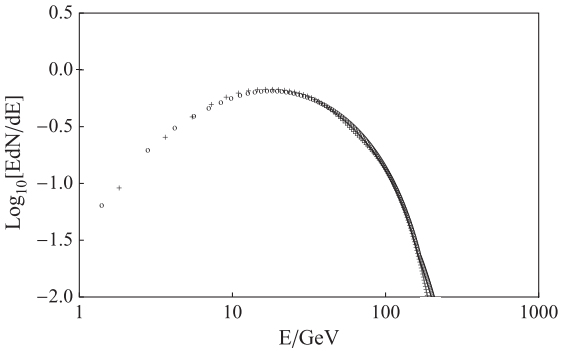

FIG. 5. The sum of the muon neutrino and antineutrino spectrum from nuclear collisions, calculated in the stellar frame using the numerical method A (curve marked by "+") and the method B (curve marked by "o"), as discussed in Sec. III A. Both spectra are normalized to one pp collision event. In the outer jet comoving frame (where target protons are at rest), the incident proton kinetic energy is $T_p = 3.8$ GeV. In the case shown here, the outer jet Lorentz factor is $\eta_{\rm out} = 70$, and the inner jet's is $\eta_{\rm core} = 700$.

As discussed in Sec. II, most of these neutrinos come from transverse drift collisions rather than from radial drifts. We have used parameters representative of standard long GRB, extending from moderate to high intrinsic luminosity, and the fluence is calculated for a nominal redshift of $z = 0.1$, corresponding to a luminosity distance of 450 Mpc in a standard $\Omega_m = 0.28$, $\Omega_V = 0.72$, $h = 0.72$ cosmology. This is at the lower end of the classical redshift distribution, since for the 5–100 GeV neutrino energies considered here, only rare, very nearby bursts might be expected to be detectable individually, due to the detector effective area decreasing with energy decreasing. The typical neutrino fluences in Figs. 2–4 are $\lesssim$ GeV cm$^{-2} \sim 1.6 \times 10^{-3}$ erg cm^{-2} for $z = 0.1$. Since pp collisions are expected to produce a comparable amount of energy in photons from π^0 decay as in neutrinos, it is important to check that such a photon luminosity[6] does not violate electromagnetic observation constraints. There are no gamma-ray detections at TeV energies so far, and the smattering of GeV detections involve bursts typically at much higher redshifts than considered here, so the possible constraints are mainly the 20–300 keV energy range fluence statistics from the BATSE 4B [35] compilation of bursts. We can conservatively assume that, at most, a fraction $\lesssim 0.3$ of the total π^0 photon energy will appear in the 20–300 keV range, i.e. $\lesssim 5 \times 10^{-4}$ erg cm^{-2}. Such fluences are marginally compatible with the BATSE 4B statistics, which does include some objects with fluences $\lesssim 10^{-3}$ erg/cm^2 (BATSE does not provide redshift information, but it is known that most BATSE bursts are at $z \gtrsim 1$; here, we considered our bursts at $z < 0.1$, and if these were placed at the typical $z > 1$, they would show a BATSE fluence $\lesssim 5 \times 10^{-6}$ erg cm^{-2}). Thus, our electromagnetic fluences appear compatible with the current observations.

The number of muon events arising from the above incident muon neutrino and antineutrino fluences is calculated based on the specific detector characteristics. For the IceCube full 86-string operation, the effective area is larger than that of DeepCore at $\sim$100 GeV, and these effective areas being given by Ref. [25]. For a detection relying exclusively on neutrinos, one would need to consider GRBs which show at least one muon event. However, bursts able to give an average of >0.01 muon events are also of interest because of the expectation of natural fluctuations in the distance or in the luminosity and because, in some cases, temporally coincident electromagnetic observations can be expected. The burst values of L_γ and redshift z yielding different muon event numbers for different burst parameters are shown by the contours in Fig. 6.

The average rate per year at which GRBs occur producing ≥ 1 muon events can be estimated using the GRB luminosity and redshift distributions discussed in Sec. III B. For a baryon-to-photon luminosity ratio of 10, i.e. $\epsilon_b = 10\epsilon_e \approx 1$, with inner-to-outer-jet Lorentz factor contrasts of $\eta_{\rm core} = 10\eta_{\rm out} = 300$, 700, 1000, respectively, this average rate is expected to be around 0.0006/yr, 0.04/yr and 0.06/yr.

B. Diffuse neutrino flux

The diffuse neutrino flux from all GRBs in the sky can be calculated using a GRB luminosity distribution (luminosity function) and a redshift distribution.[7] Here, we adopt for these the functions given in Ref. [37]

$$\phi(L_\gamma) \propto \begin{cases} (L_\gamma/L_*)^{m_1} & L_{\rm min} < L_\gamma < L_* \\ (L_\gamma/L_*)^{m_2} & L_* < L_\gamma < L_{\rm max} \end{cases} \tag{18}$$

$$R_{\rm GRB}(z) \propto \begin{cases} (1+z)^{n_1} & z < z_1 \\ (1+z)^{n_2} & z > z_1 \end{cases}. \tag{19}$$

Here, Eq. (18) is the luminosity function, and Eq. (19) is the redshift distribution function, L_γ is the peak photon luminosity (typically in the 0.1–0.3 MeV range), $L_{\rm min} = 10^{50}$ erg/s, $L_* = 10^{52.5}$ erg/s, $L_{\rm max} = 10^{54}$ erg/s, $m_1 = -0.2$, $m_2 = -1.4$, $n_1 = 1.0$, $n_2 = -1.4$, $z_1 = 3$, and we have used these values from the [37] parameter ranges which best reproduce the actual GRBs with measured L_γ and z statistics, e.g. Fig. 2 of Ref. [37], Fig. 4 of Ref. [38], or Ref. [39]. We note that, especially in the range $z \lesssim 0.5$, the index of the redshift distribution, i.e. the rate, is very

[6] An evaluation of the final photon spectrum would require the use of a detailed electromagnetic cascade code, which is beyond the scope of this paper.

[7] For the method of calculation, see, e.g., Appendix B of Ref. [36].

uncertain due to poor statistics. The differential comoving rate of GRBs at a redshift z is given by

$$R(z) = \frac{R_{\rm GRB}(z)}{(1+z)} \frac{dV(z)}{dz}, \tag{20}$$

where $V(z)$ is the comoving volume in the ΛCDM cosmology model adopted, with $\Omega_m = 0.28$, $\Omega_V = 0.72$ and $H_0 = 72$ Km/s/Mpc. The differential number of GRB per unit redshifts is given by

$$dN = \rho_0 \phi(L_\gamma) R(z) d\log L_\gamma dz, \tag{21}$$

where ρ_0 is the normalization factor. In this paper, we normalize the total electromagnetically detected GRB rate to 300/yr in the range given by Eqs. (18) and (19). The neutrino flux depends on the baryon luminosity L_b, and the ratio between L_b and L_γ adopted in Sec. III A is $L_b/L_\gamma \approx 10$. This ratio is characteristic of many hadronic GRB models, the implied photon radiative efficiency of 10% being moderate. The resulting diffuse neutrino fluxes (neutrinos per year) are shown in Fig. 7 and are discussed in Sec. IV.

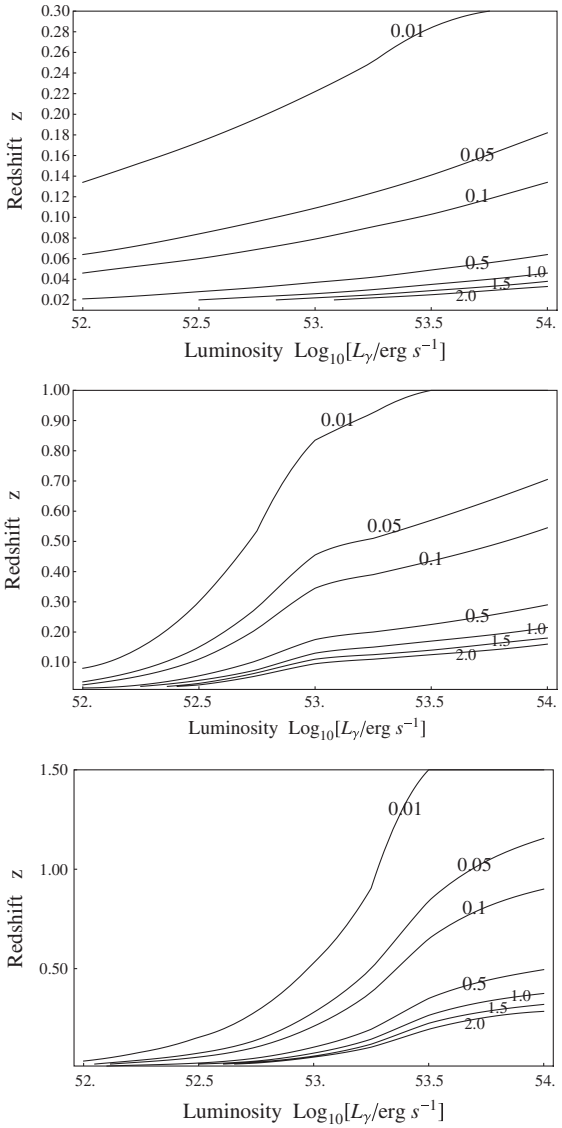

FIG. 6. Expected number of muon events in the full 86-strings IceCube and its DeepCore subarray, from a *single GRB* with $\eta_{\rm core} = 10\eta_{\rm out} = 300$ (top panel), 700 (middle panel), 1000 (bottom panel), from various redshifts z and for different photon luminosities L_γ, assuming a baryon-to-photon luminosity ratio of 10, or $\epsilon_b = 2\epsilon_p \sim 10\epsilon_\gamma$. The effective detection areas are taken from Ref. [25], with the angular position averaged over the northern sky (the effective areas have some dependence on the incident angle of the neutrinos). These contours show the L_γ and z ranges which give 0.02–2 muon events.

IV. DISCUSSION

We have calculated the neutrino emission in the range of a few GeV to a few hundred GeV arising in magnetized collisional GRB models, such as have been recently used for interpreting the electromagnetic properties of these objects. The neutrino emission considered here arises partly from longitudinal proton and neutron collisions following their decoupling in the jet, and in larger part, from collisions caused by transverse thermal drift of neutrons from an outer jet sheath into the jet core, having different bulk Lorentz factors. This neutrino production model differs from the commonly considered photohadronic $p\gamma$ models, and it also differs from previous pn model calculations in incorporating explicitly the (dominant) transverse drift collision effects. Also, the emission region characteristics are here determined by the magnetically dominated dynamics, differing from those in previous neutrino calculations, which mostly use baryonic dynamics. Furthermore, the pn neutrino spectra are calculated numerically, using two different codes which are suited for the GeV range energies considered.

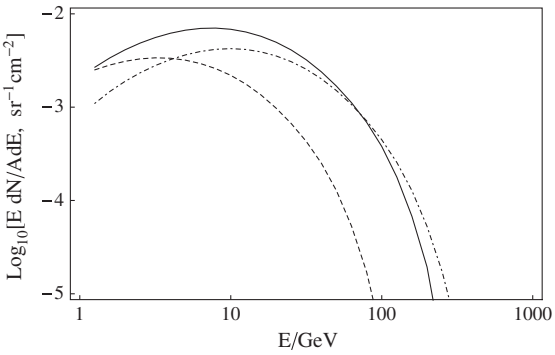

FIG. 7. The diffuse muon neutrino and antineutrino fluence per year (after oscillations) for all GRBs down to $z > 0.01$, as discussed in Sec. IV, using the luminosity function and redshift distribution of Sec. III B. The conventions and parameters are the same as in Fig. 6, except for using $\eta_{\rm core} = 10\eta_{\rm out} = 300$ (dashed), 700 (solid) and 1000 (dotted-dashed).

Our present results indicate that for the burst parameters suitable to explain the photon spectra and the MeV–GeV photon lags [23] indicated by the recent Fermi satellite observations, a low level of neutrino emission is expected at ~5–100 GeV energies. This is in the sensitivity range of the DeepCore subarray of IceCube and extends into the lower range of the main IceCube array.

For a neutrino detection of an individual burst, unaided by a coincident electromagnetic detection, one would require $\gtrsim 1$ muon event. For neutrino-induced muon track events in IceCube and DeepCore, considering the angular resolution (e.g. $\Omega \lesssim 10^2$ deg^2) and time search bins $\sim o(1) \times 20$ s per burst, the atmospheric neutrino background is low. During the total sum of the search bins (e.g. assuming 300 electromagnetically observed long GRBs in a year) from the atmospheric neutrino spectrum, the expected number of background muon events is $\lesssim o(1) \times 0.09$.

However, any GRBs which might be expected to yield $\gtrsim 1$ muon event need to be at the high end of the luminosity function and located at very low redshifts, $L_{\gamma,\mathrm{iso}} \gtrsim 10^{53}$ erg/s and $z \lesssim 0.1$. From the discussion of Sec. III B, the occurrence of such GRB is estimated to be very rare, $\lesssim 1/17$ per year. This estimate is uncertain, because of the poor statistics in the determination of the redshift distribution in this range. Such bursts would in general also be detectable by photon detectors such as Swift and Fermi, except for Earth occultations or possible outages. For the more frequent weaker or more distant bursts, taking into account fluctuations in the average quantities, a neutrino observation correlated with a photon detection can narrow the time bin search, increasing the effective sensitivity of the detection. The rate of occurrence of such lower fluence GRBs can be calculated from the luminosity function and redshift distribution, and is shown in Fig. 6).

Because of the low occurrence rate of bursts which can be expected to be detected individually, it is useful to consider also the diffuse neutrino fluxes. The same luminosity function and redshift distribution as above were used for this, as discussed in Sec. III B, extending the integration to all bursts with $z \geq 0.01$. In Fig. 7, we show the diffuse neutrino fluences over the period of a year, for a set of burst parameters $\eta_{\mathrm{core}} = 10\eta_{\mathrm{out}} = 300$, 700, 1000 and $\epsilon_b = 10\epsilon_e \approx 1$. For these parameters, the corresponding number of average expected muon events in IceCube and its DeepCore array are estimated to be 0.03, 0.4 and 0.5 per year over the whole sky, respectively. Because of the poor statistics in the rate of low redshift GRBs, the uncertainty in these numbers could be a factor of ~2. The IceCube IC40 + IC59 muon event rates per year being used to set upper limits on the TeV–PeV neutrino flux from putative Waxman-Bahcall GRB models (different from the present model) are larger than the event rates discussed here, but within 1 order of magnitude of those for the highest η values. Thus, imposing weak limits may be possible in the long term.

In conclusion, both the individual burst fluences and the expected diffuse flux in the 5–100 GeV range are significantly low. Fortuitous fluctuations above the mean values could increase this somewhat, but any conclusions based on the current IceCube and DeepCore arrays are likely to require years of data accumulation with the full array. The proposed upgrades to these installations would help, but a next generation of larger effective volume neutrino detectors could be the best way to accelerate the detection or nondetection of GRB neutrinos in this energy range and to test GRB models such as discussed here.

ACKNOWLEDGMENTS

We thank P. Veres, M. Strikman, M. Smith, D. Cowen and especially T. DeYoung for useful discussions, the referee for valuable critical comments, and NASA (NNX09AL40G) and NSF (PHY-0757155) for partial support.

[1] A. A. Abdo and Fermi Collaboration, Science **323**, 1688 (2009).
[2] M. Ackermann and Fermi Collaboration, Astrophys. J. **716**, 1178 (2010).
[3] A. Pe'er, in 2011 Fermi Symposium Proceedings, Rome, 2011 (unpublished).
[4] P. Mészáros and M. Rees, Astrophys. J. **530**, 292 (2000).
[5] M. J. Rees and P. Mészáros, Astrophys. J. **628**, 847 (2005).
[6] A. M. Beloborodov, Mon. Not. R. Astron. Soc. (to be published).
[7] E. V. Derishev, V. V. Kocharovsky, and V. V. Kocharovsky, Astrophys. J. **521**, 640 (1999).
[8] J. N. Bahcall and P. Mészáros, Phys. Rev. Lett. **85**, 1362 (2000).
[9] P. Mészáros and M. J. Rees, Astrophys. J. Lett. **541**, L5 (2000).
[10] D. Giannios and H. C. Spruit, Astron. Astrophys. **469**, 1 (2007).
[11] A. Tchekhovskoy, R. Narayan, and J. C. McKinney, New Astron. Rev. **15**, 749 (2010).
[12] P. Mészáros and M. Rees, Astrophys. J. **715**, 967 (2010).
[13] V. V. Usov, Mon. Not. R. Astron. Soc. **267**, 1035 (1994).
[14] P. Mészáros and M. J. Rees, Astrophys. J. Lett. **482**, L29 (1997).

[15] K. Toma, T. Sakamoto, and P. Mészáros, Astrophys. J. **731**, 127 (2011).
[16] S. Gao, K. Toma, and P. Mészáros, Phys. Rev. D **83**, 103004 (2011).
[17] C. Thompson, Mon. Not. R. Astron. Soc. **270**, 480 (1994).
[18] G. Drenkhahn and H. C. Spruit, Astron. Astrophys. **391**, 1141 (2002).
[19] M. Lyutikov and R. Blandford, arXiv:astro-ph/0312347.
[20] J. C. McKinney and D. A. Uzdensky, Mon. Not. R. Astron. Soc. (to be published).
[21] B. D. Metzger, D. Giannios, T. A. Thompson, N. Bucciantini, and E. Quataert, Mon. Not. R. Astron. Soc. **413**, 2031 (2011).
[22] H. B. J. Koers and D. Giannios, Astron. Astrophys. **471**, 395 (2007).
[23] P. Mészáros and M. Rees, Astrophys. J. Lett. **733**, L40 (2011).
[24] T. DeYoung for the IceCube Collaboration, arXiv:1112.1053.
[25] The IceCube Collaboration., arXiv:1109.6096.
[26] The IceCube Collaboration, in 32nd International Cosmic Ray Conference, Beijing, 2011 (unpublished).
[27] G. Drenkhahn, Astron. Astrophys. **387**, 714 (2002).
[28] J. Granot, Mon. Not. R. Astron. Soc. (to be published).
[29] B. D. Metzger, D. Giannios, and S. Horiuchi, Mon. Not. R. Astron. Soc. **415**, 2495 (2011).
[30] W. Zhang, S. E. Woosley, and A. I. MacFadyen, Astrophys. J. **586**, 356 (2003).
[31] A. Tchekhovskoy, J. C. McKinney, and R. Narayan, Mon. Not. R. Astron. Soc. **388**, 551 (2008).
[32] T. Kamae, N. Karlsson, T. Mizuno, T. Abe, and T. Koi, Astrophys. J. **647**, 692 (2006).
[33] A. M. Hillas, in *16th International Cosmic Ray Conference*, International Cosmic Ray Conference Vol. 6 (Institute for Cosmic Ray Research, University of Tokyo, Tokyo, 1979), p. 13.
[34] A. P. Marscher, W. T. Vestrand, and J. S. Scott, Astrophys. J. **241**, 1166 (1980).
[35] W. S. Paciesas, C. A. Meegan, G. N. Pendleton, M. S. Briggs, C. Kouveliotou, T. M. Koshut, J. P. Lestrade, M. L. McCollough, J. J. Brainerd, J. Hakkila, W. Henze, R. D. Preece, V. Connaughton, R. M. Kippen, R. S. Mallozzi, G. J. Fishman, G. A. Richardson, and M. Sahi, Astrophys. J. Suppl. Ser. **122**, 465 (1999).
[36] K. Murase, Phys. Rev. D **76**, 123001 (2007).
[37] D. Wanderman and T. Piran, Mon. Not. R. Astron. Soc. **406**, 1944 (2010).
[38] N. Gehrels, E. Ramirez-Ruiz, and D. B. Fox, Annu. Rev. Astron. Astrophys. **47**, 567 (2009).
[39] J. Greiner, http://www.mpe.mpg.de/~jcg/grbgen.html (2011).